Observations of the Large Magellanic Cloud with Fermi

J. Knödlseder and P. Jean
Centre d'Étude Spatiale des Rayonnements, CNRS/UPS, BP 44346, F-31028 Toulouse Cedex 4, France
on behalf of the Fermi/LAT Collaboration

We report on observations of the Large Magellanic Cloud with the Fermi Gamma-Ray Space Telescope. The LMC is clearly detected with the Large Area Telescope (LAT) and for the first time the emission is spatially well resolved in gamma-rays. Our observations reveal the massive star forming region 30 Doradus as a bright source of gamma-ray emission in the LMC. The observations furthermore show that the gamma-ray emission correlates little with the gas density of the LMC. Implications of this finding will be discussed.

1. Introduction

Since the early days of high-energy gamma-ray astronomy it has been clear that the gamma-ray flux received at Earth is dominated by emission from the Galactic disk [1]. This emission is believed to arise from cosmic-ray interactions with the interstellar medium, which at gamma-ray energies $\gtrsim 100$ MeV are dominated by the decay of π^0 produced in collisions between cosmic-ray nuclei and the interstellar medium [2]. Further contributions are from cosmic-ray electrons undergoing inverse Compton scattering off interstellar soft photons and Bremsstrahlung losses within the interstellar medium. Gamma-ray observations thus have the potential to map cosmic-ray acceleration sites in our Galaxy which may ultimately help to identify the sources of cosmic-ray acceleration.

Nearby galaxies have the advantage of being viewed from outside and so line of sight confusion, which complicates studies of emission from the Galactic disk, is diminished. This advantage is however somewhat offset by the limitations by the angular resolution and sensitivity of the instrument. The Large Magellanic Cloud (LMC) is thus an excellent target for studying the link between cosmic-ray acceleration and gamma-ray emission since the galaxy is nearby ($D \approx 50$ kpc) [3, 4], has a large angular extent of $\sim 8°$, and is seen at a small inclination angle of $i \approx 20° - 35°$ [5, 6] that avoids source confusion. In addition, the LMC is relatively active, housing many supernova remnants, bubbles and superbubbles, and massive star forming regions that are all potential sites of cosmic-ray acceleration [7, 8, 9].

The EGRET telescope onboard the Compton Gamma-Ray Observatory (*CGRO*, 1991–2000) was the first to detect the LMC [10]. Due to EGRET's limited angular resolution and limited sensitivity, details of the spatial structure of the gamma-ray emission could not be resolved, yet the observations showed some evidence for the spatial distribution being consistent with the morphology of radio emission. The Large Area Telescope (LAT) aboard *Fermi* is providing now for the first time the capabilities to go well beyond the study of the integrated gamma-ray flux from the LMC [11, 12]. In this contribution we present our first in-depth analysis of the LMC galaxy based on 11 months of continuous sky survey observations performed with *Fermi*/LAT. We put a particular emphasis on the determination of the spatial distribution of the gamma-ray emission, that, as we will show, reveals the distribution of cosmic rays in the galaxy. A more detailed discussion of the observations and their implications is given in [13].

2. Observations

2.1. Data preparation

The characteristics and performance of the LAT aboard *Fermi* are described in detail by [15]. The data used in this work amount to 274.3 days of continuous sky survey observations over the period August 8th 2008 – July 9th 2009 during which a total exposure of $\sim 2.5 \times 10^{10}$ cm^2 s (at 1 GeV) is obtained for the LMC. Events satisfying the standard low-background event selection ("Diffuse" events) [15] and coming from zenith angles $< 105°$ (to greatly reduce the contribution by Earth albedo gamma rays) are used. To further reduce the effect of Earth albedo backgrounds, the time intervals when the Earth was appreciably within the field of view (specifically, when the center of the field of view was more than 47° from the zenith) are excluded from this analysis. Furthermore, time intervals when the spacecraft was within the South Atlantic Anomaly are also excluded. We further restrict the analysis to photon energies above 200 MeV; below this energy the effective area in the "Diffuse class" is relatively small and strongly dependent on energy. All analysis is performed using the LAT Science Tools package, which is available from the Fermi Science Support Center, using P6_V3 post-launch instrument response functions (IRFs). These take into account pile-up and accidental coincidence effects in the detector subsystems that are not considered in the definition of the pre-launch IRFs.

At the Galactic latitude of the LMC ($b \approx -33°$), the gamma-ray background is a combination of ex-

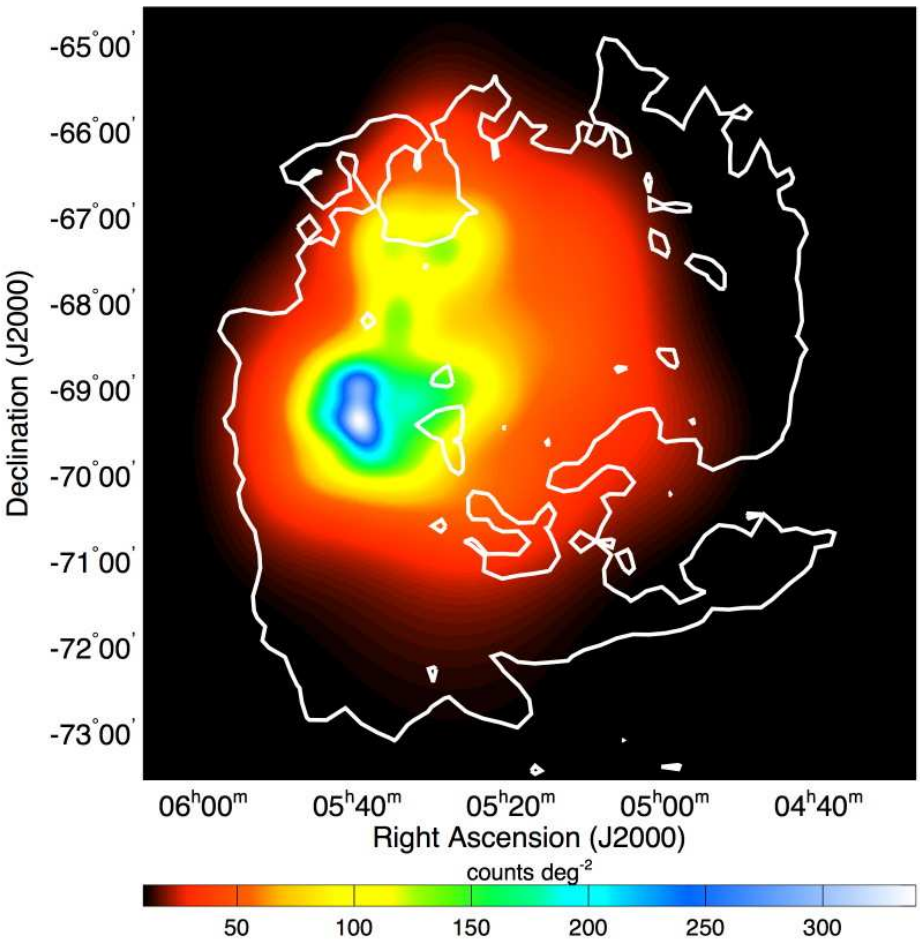

Figure 1: Background subtracted counts map of the LMC region. The counts map has been adaptively smoothed [14] with a signal-to-noise ratio of 5 in order to reveal significant structures at all possible scales while supressing the noise that arises from photon counting statistics. The white line shows the N(H I) = 10^{21} H cm^{-2} iso column density contour to indicate the extent of the gaseous disk.

tragalactic and Galactic diffuse emissions, some residual instrumental background and a number of point sources that primarily are associated to blazars. We model the background using components for the diffuse Galactic and the extragalactic and residual instrumental backgrounds and 6 point sources that all are associated with known blazars. The Galactic component is based on the LAT standard diffuse background model `gll_iem_v02` for which we keep the overall normalization as a free parameter. The extragalactic and residual instrumental backgrounds are combined into a single component which has been taken as being isotropic. The spectrum of this component is determined by fitting an isotropic component together with a model of the Galactic diffuse emission and point sources to the data. Also here we leave the overall normalization of the component as a free parameter. The 6 background blazars are modelled as point sources with power-law spectral shapes. The flux and spectral power-law index of each source are left as free parameters of our background model and their values were determined from likelihood analysis.

2.2. Spatial distribution

2.2.1. Counts map

To investigate the spatial distribution of gamma-ray emission toward the LMC we show in Fig. 1 an adaptively smoothed background subtracted counts map of the LAT data. The map clearly shows extended emission that is spatially confined to within the LMC boundaries which we trace by the iso column density contour $N_{\rm H}$ = 10^{21} H cm^{-2} of neutral hydrogen in the LMC [16]. The total number of excess 200 MeV – 20 GeV photons above the background

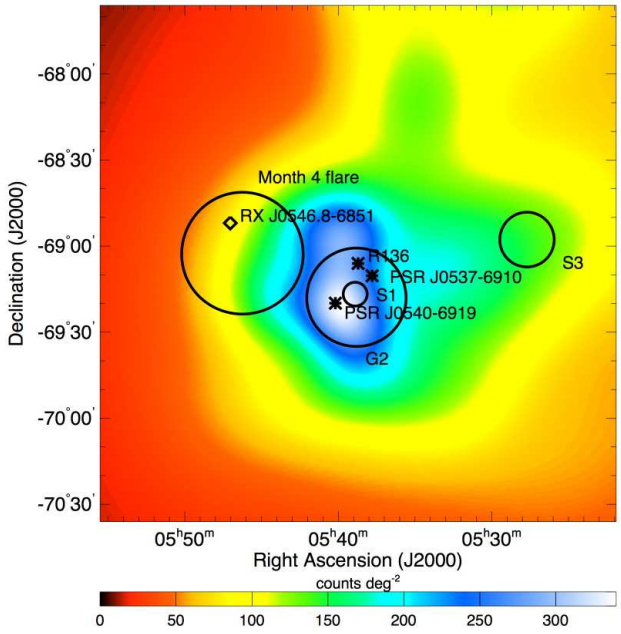

Figure 2: Zoom into a $3^\circ \times 3^\circ$ large region of the background subtracted counts map around the central star cluster R 136 in 30 Dor. Stars show the locations of R 136 and of the pulsars PSR J0540−6919 and PSR J0537−6910. The circles show the 95% containment radius of sources S1 and S3 of the point source model, and of source G2 of the 2D Gaussian shaped model (see text). During month 4 of our dataset, a flaring point source occured near 30 Dor, and we indicate the 95% containment radius of this source; the diamond shows the location of the possible counterpart RX J0546.8−6851 of the flaring source.

in the LMC area amounts to ~ 1550 counts whereas the background in the same area amounts to ~ 2440 counts. With these statistics, the extended gamma-ray emission from the LMC can be resolved into several components. The brightest emission feature is located near $(\alpha_{\rm J2000}, \delta_{\rm J2000}) \approx (05^{\rm h}40^{\rm m}, -69°15')$, which is close to the massive star-forming region 30 Doradus (30 Dor) that houses the two Crab-like pulsars PSR J0540−6919 and PSR J0537−6910 [17, 18]. Excess gamma-ray emission is also seen toward the north and the west of 30 Dor. These bright regions are embedded into a more extended and diffuse glow that covers an area of approximately $5^\circ \times 5^\circ$. Figure 2 present a zoom of Fig. 1 of the 30 Dor region over which we overlay potential sources of gamma-ray emission.

2.2.2. Model fitting

As next step, we assess the spatial distribution of the LMC emission using (1) simple parametrized geometrical models of the gamma-ray intensity distribution, and (2) spatial templates that trace the interstellar matter distribution in the LMC. We assume power-law spectral distributions for all models and keep the total flux and power law index as free parameters. We adjust the spatial and spectral parameters of the models using a binned maximum likelihood analysis with spatial bins of $0.1^\circ \times 0.1^\circ$ and 60 logarithmically spaced energy bins covering the energy range 200 MeV – 20 GeV. We quantify the goodness-of-fit using the so-called *Test Statistic* (TS) which is defined as twice the difference between the log-likelihood $\mathcal{L}_1$ that is obtained by fitting the model on top of the background model to the data, and the log-likelihood $\mathcal{L}_0$ that is obtained by fitting the background model only, i.e. $\mathrm{TS} = 2(\mathcal{L}_1 - \mathcal{L}_0)$.

First, we examine if the gamma-ray emission from the LMC can be explained with a combination of individual point sources. For this purpose we add successive point sources to our model and optimize their locations, fluxes and spectral indices by maximizing the likelihood of the model. We stop this procedure once the TS improvement after adding a further point source drops below 25. This happens after we added 5 point source to our model, resulting in TS = 1089.3. The left panel of Fig. 3 shows the corresponding model counts map.

Second, instead of using point sources we repeat the procedure with 2D Gaussian shaped intensity profiles to build a geometrical model that is more appropriate for extended and diffuse emission structures. We again stop the successive addition of 2D Gaussian shaped sources once the TS improvement after adding a further source drops below 25. This occurs after two 2D Gaussian shaped sources have been added to the model, resulting in TS = 1122.6. We show the corresponding model counts map in the right panel of Fig. 3. Obviously, the 2D Gaussian model provides a larger TS than the point source model, suggesting that it better fits the data despite the smaller number of free parameter (10 for the 2D Gaussian model compared to 20 for the point source model). It is thus more likely that the LMC emission is indeed diffuse in nature, or alternatively, composed of a large number of unresolved and faint sources that can not be detected individually by *Fermi*/LAT.

Third, we fit the LAT data to gas maps of neutral atomic hydrogen (H I) [16], molecular hydrogen (H_2) [19], and ionized hydrogen (H II) [20]. Fitting the H I and H_2 maps result in TS values of 771.8 and 824.3, respectively, that are considerably worse than those obtained for the geometrical models. Apparently, the H I and H_2 maps provide rather poor fits to the data, indicating that the distribution of gamma rays does not follow the distribution of neutral hydrogen in the LMC. This can already be seen from the left and mid panels of Fig. 4 which show the gas maps after convolution with the LAT point spread function. While the gamma-ray emissivity is highest in 30 Dor and the northern part of the galaxy,

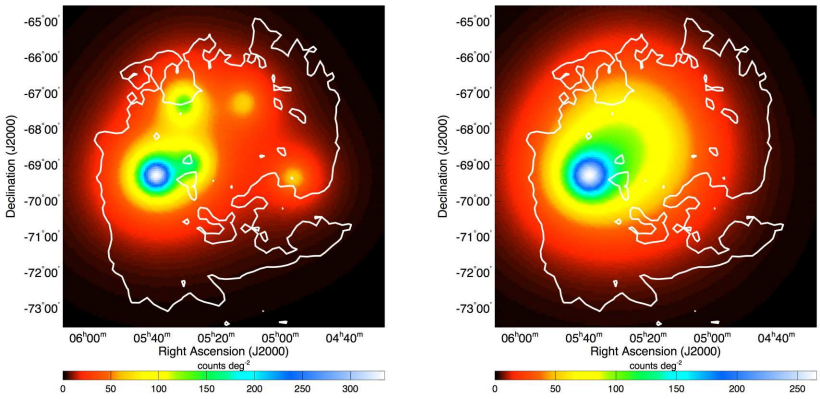

Figure 3: Best fitting point source model (left panel) and 2D Gaussian shape model (right panel) that has been convolved with the LAT point spread function. The point source model consists of 5 point sources (S1-S5) while the 2D Gaussian shaped model consists of a broad component covering a large fraction of the LMC disk (G1) and a narrow component near 30 Dor (G2).

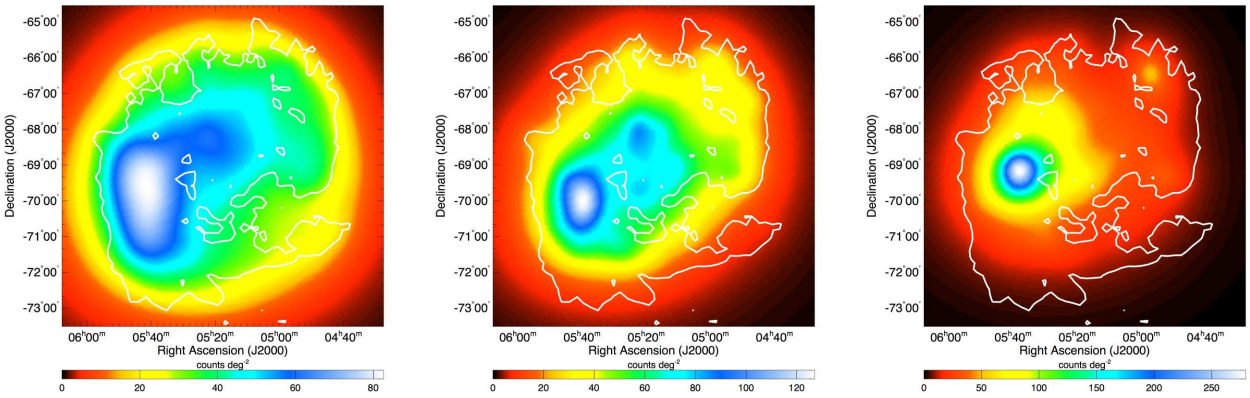

Figure 4: Gas tracer maps convolved with the LAT point spread function and scaled using maximum likelihood model fitting to the data. Panels show H I (left panel), H_2 (mid panel), and H II (right panel).

the gas maps show a bright ridge that runs over $\sim 3^\circ$ along $\alpha_{\rm J2000} \sim 05^{\rm h}40^{\rm m}$ which coincides with the most prominent region of ^{12}CO emission tracing giant molecular clouds in the LMC [21]. Roughly 20% of the total gas mass in the LMC is confined into this ridge [22], yet comparison with Fig. 1 shows that most of the ridge is not luminuous in high-energy gamma rays.

The H II map, on the other hand, gives TS = 1110.1, which is very close to the TS values of the geometrical models. The H II map thus provides the best fit among all of the gas maps to the LAT data, and the right panel of Fig. 4 indeed shows that the model is very similar to the 2D Gaussian shaped model and also follows closely the observed distribution of gamma rays (Fig. 1).

2.3. Emissivity spectrum

To determine the spectrum of the gamma-ray emission from the LMC independently from any assumption on the spectral shape, we fit our data in 6 logarithmically spaced energy bins covering the energy range 200 MeV - 20 GeV. We obtain the total spectrum of the LMC by fitting the H II template to the data. We also obtain separate spectra for the LMC disk (G1) and for 30 Dor (G2) by fitting the 2D Gaussian shaped model to the data.

To determine the integrated gamma-ray flux we fit exponentially cut off power law spectral models of the form $N(E) = k\,(E/E_0)^{-\Gamma} \exp(-E/E_{\rm c})$ to the data. We make these fits by means of a binned maximum likelihood analysis over the energy range 200 MeV - 20 GeV. This results in an extrapolated > 100 MeV photons flux of $(2.6 \pm 0.2) \times 10^{-7}$ ph cm^{-2} s^{-1} for the H II template which corresponds to an energy flux of $(1.6 \pm 0.1) \times 10^{-10}$ erg cm^{-2} s^{-1} (systematic uncer-

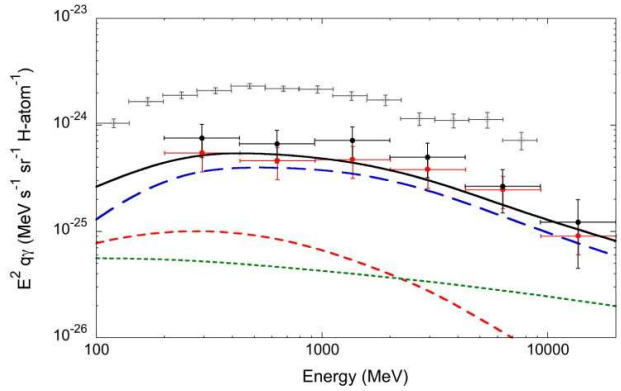

Figure 5: Differential average gamma-ray emissivity for the total LMC emission (black dots) and for the LMC disk only (red dots) compared to that of the Galactic local interstellar medium determined by [23] (grey data points). The solid line shows the predicted gamma-ray emissivity computed in the framework of a one-zone model for the LMC disk [13]. The other lines show the contributions of π^0-decay (long dashed), Bremsstrahlung (short dashed), and inverse Compton emission (dotted).

tainties in these estimates amount to less than 16%).

Dividing our spectra by the spatially integrated hydrogen column density $\int N_{\rm H}\,{\rm d}\Omega = (3.6\pm1.2)\times10^{19}$ H-atom cm^{-2} sr of the LMC provides us with the differential gamma-ray emissivity per hydrogen atom. We compare the resulting emissivity for the total LMC emission and the LMC disk only in Fig. 5 to the one obtained for the Galactic local interstellar medium by [23]. Apparently, the local Galactic emissivity is between ~ 2 to ~ 4 times larger than the average emissivity of the LMC.

We compare the differential gamma-ray emissivities to a one-zone model of cosmic-ray interactions with the interstellar medium that takes into account π^0 decay following proton-proton interactions, Bremsstrahlung from cosmic-ray electrons and inverse Compton scattering of cosmic-ray electrons on LMC optical and infrared photons and cosmic microwave background photons [13]. Fitting this spectral model to our data using a binned maximum likelihood analysis gives an average cosmic-ray enhancement factor of $r_c = 0.31 \pm 0.01$ for the entire LMC, and of $r_c = 0.21 \pm 0.01$ for the LMC disk only. Systematic errors due to uncertainties in the effective area of the instrument amount to ±0.02. An additional systematic error of -23% to $+42\%$ comes from the uncertainty in the total gas mass of the LMC, which largely dominates the statistical and systematic measurements errors.

3. Cosmic-ray density distribution

To reveal the sites of cosmic-ray acceleration in the LMC we map the cosmic-ray density variations in the galaxy by computing the gamma-ray emissivity as function of position. We do this by dividing our background subtracted counts map by the N(H) map after convolution of the latter with the LAT instrumental response function. We normalise N(H) to a total LMC hydrogen mass of $7.2\times10^8\ M_\odot$ that takes into account the possible presence of dark gas that is not seen in radio surveys of H I [27]. We adaptively smooth [14] the counts maps and used the resulting smoothing kernel distribution to smooth also the convolved N(H) map before the division to reveal significant structures at all possible scales, while supressing the noise that arises from the limited photon counting statistics. The resulting emissivity maps are shown in Fig. 6. We superimpose on the images the interstellar gas distribution, as traced by N(H), convolved with the LAT instrumental response function, and also show the locations of potential particle acceleration sites, such as pulsars, supernova remnants, Wolf-Rayet stars and supergiant shells.

Figure 6 reveals that the cosmic-ray density varies considerably over the disk of the LMC. The gamma-ray emissivity is highest in 30 Dor and the northern part of the galaxy, while the southern part and in particular the dense ridge of gas south of 30 Dor seems basically devoid of cosmic rays. These large variations confirm our earlier findings that the gamma-ray emission correlates little with the gas density in the LMC. Figure 6 suggests further that the cosmic-ray density correlates with massive star forming tracers, and in particular Wolf-Rayet stars and supergiant shells. This finding is corroborated by the good fit of the H II gas map, which is probably the most direct tracer of massive star forming regions within a galaxy.

Thus, the gamma-ray emissivity maps of the LMC support the idea that cosmic rays are accelerated in massive star forming regions as a result of the large amounts of kinetic energy that are input by the stellar winds and supernova explosions of massive stars into the interstellar medium. Our data reveal a relatively tight confinement of the gamma-ray emission to star forming regions, which suggests a relatively short diffusion length for GeV protons.

4. Conclusions

Observations of the LMC by *Fermi*/LAT have for the first time provided a detailed map of high-energy gamma-ray emission from that galaxy. Our analysis reveals the massive star forming region 30 Doradus as bright source of gamma-ray emission in the LMC in addition to fainter emission regions found in the northern part of the galaxy. The gamma-ray emission from

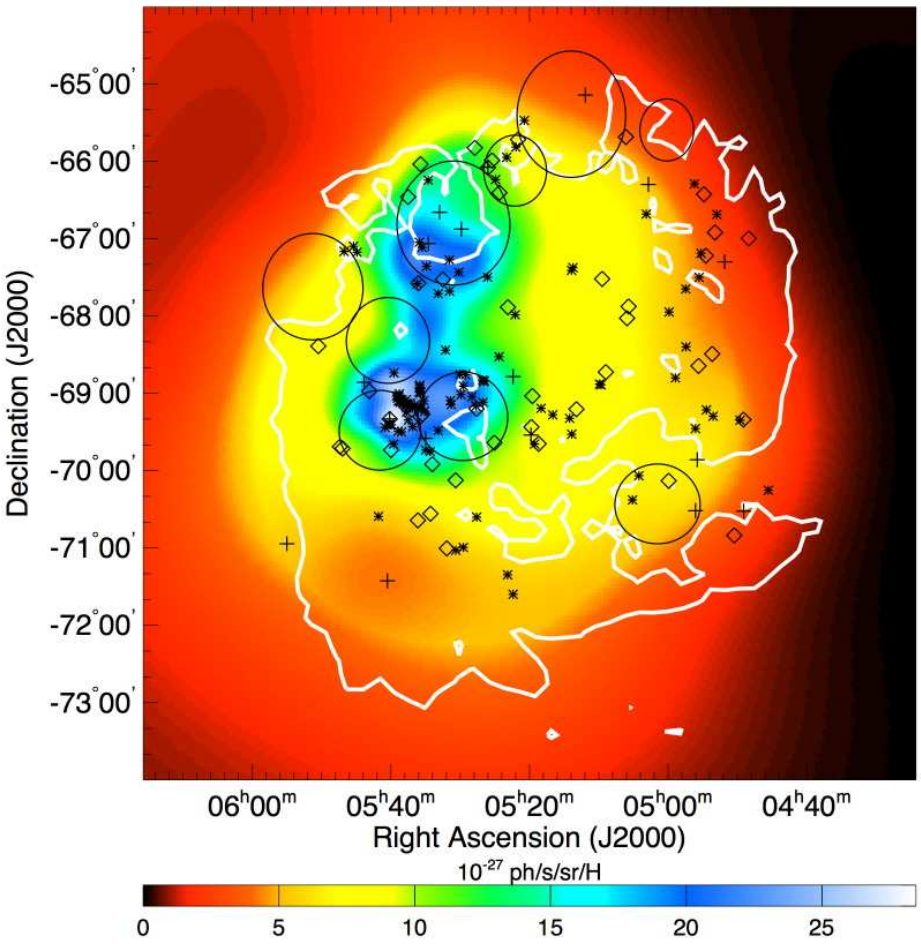

Figure 6: Integrated > 100 MeV emissivity maps of the LMC in units of 10^{-27} ph s^{-1} sr^{-1} H-atom^{-1}. An adaptive smoothing with a signal-to-noise ratio of 5 has been applied to reduce statistical fluctuations. The white line shows the N(H I) = 10^{21} H cm^{-2} iso column density contour to indicate the extent of the gaseous disk. Symbols indicate the locations of pulsars (pluses) from ATNF catalogue version 1.36 [24], supernova remnants (diamonds) from Rosa Williams web page http://www.astro.illinois.edu/projects/atlas/index.html, Wolf-Rayet stars (stars) from the fourth catalogue of [25], and supergiant shells (circles) from [26].

the LMC shows very little correlation with gas density. A much better correlation is seen between gamma-ray emission and massive star forming regions, as traced by the ionizing gas, Wolf-Rayet stars and supergiant shells, and we take this as evidence for cosmic-ray acceleration in these regions. This correlation supports the idea that cosmic rays are accelerated in massive star forming regions as a result of the large amounts of kinetic energy that are input by the stellar winds and supernova explosions of massive stars into the interstellar medium.

Continuing observations of the LMC with *Fermi*/LAT in the upcoming years will provide the photon statistics to learn more about the origin of the gamma-ray emission from that galaxy. Better statistics will help in identifying more individual emission components and may help to separate true point sources from the more diffuse emission that we expect from cosmic-ray interactions.

Acknowledgments

The *Fermi* LAT Collaboration acknowledges generous ongoing support from a number of agencies and institutes that have supported both the development and the operation of the LAT as well as scientific data analysis. These include the National Aeronautics and Space Administration and the Department of Energy in the United States, the Commissariat à l'Energie Atomique and the Centre National

de la Recherche Scientifique / Institut National de Physique Nucléaire et de Physique des Particules in France, the Agenzia Spaziale Italiana and the Istituto Nazionale di Fisica Nucleare in Italy, the Ministry of Education, Culture, Sports, Science and Technology (MEXT), High Energy Accelerator Research Organization (KEK) and Japan Aerospace Exploration Agency (JAXA) in Japan, and the K. A. Wallenberg Foundation, the Swedish Research Council and the Swedish National Space Board in Sweden.

Additional support for science analysis during the operations phase is gratefully acknowledged from the Istituto Nazionale di Astrofisica in Italy and the and the Centre National d'Études Spatiales in France.

References

[1] Clark, G.W., Garmire, G.P., & Kraushaar, W.L. 1968, ApJ, 153, 203
[2] Pollack, J.B., & Fazio, G.G. 1963, Phys. Rev., 131, 2684
[3] Matsunaga, N., Feast, M.W., & Menzies, J.W. 2009, MNRAS, 397, 933
[4] Pietrzynski, G., Thompson, I.B., Graczyk, D., et al. 2009, ApJ, 697 862
[5] Kim, S., Staveley-Smith, L., Dopita, M.A., et al. 1998, ApJ, 503, 674
[6] Van der Marel, R.P. 2006, in: The Local Group as an Astrophysical Laboratory, eds. M. Livio & T.M. Brown, Cambridge University Press, 47
[7] Cesarsky, C.J., & Montmerle, T. 1983, SSRv, 36, 173
[8] Biermann, P.L. 2004, New Astronomy Reviews, 48, 41
[9] Binns, W.R., Wiedenbeck, M.E., Arnould, M., et al. 2007, SSRv, 130, 439
[10] Sreekumar, P., Bertsch, D.L., Dingus, B.L., et al. 1992, ApJ, 400, L67
[11] Digel, S.W., Moskalenko, I., Ormes, J.F., et al. 2000, AIP, 528, 449
[12] Weidenspointner, G., Lonjou, V., & Knödlseder, J. 2007, AIP, 921, 498
[13] Abdo, A.A., Ackermann, M., Ajello, M., et al. 2010, A&A, in press
[14] Ebeling, H., White, D.A., & Rangarajan, F.V.N. 2006, MNRAS, 368, 65
[15] Atwood, W.B., Abdo, A.A., Ackermann, M., et al. 2009, ApJ, 697, 1071
[16] Kim, S., Staveley-Smith, L., Dopita, M.A., et al. 2005, ApJS, 143, 487
[17] Seward, F.D., Harnden, F.R., & Helfand, D.J. 1984, ApJ, 287, L19
[18] Marshall, F.E., Gotthelf, E.V., Zhang, W., Middleditch, J., & Wang, Q.D. 1998, ApJ, 499, L179
[19] Fukui, Y., Kawamura, A., Minamidani, T. 2008, ApJS, 178, 56
[20] Finkbeiner, D. 2003, ApJS, 146, 407
[21] Fukui, Y., Mizuno, N., Yamaguchi, R., et al. 1999, PASJ, 51, 745
[22] Luks, Th., & Rohlfs, K. 1992, A&A, 263, 41
[23] Abdo, A.A., Ackermann, M., Ajello, M., et al. 2009, ApJ, 703, 1249
[24] Manchester, R.N., Hobbs, G.B., Teoh, A., & Hobbs, M. 2005, AJ, 129, 1993
[25] Breysacher, J., Azzopardi, M., & Testor, G. 1999, A&AS, 137, 117
[26] Staveley-Smith, L., Kim, S., Calabretta, M.R., Haynes, R.F., & Kesteven, M.J. 2003, MNRAS, 339, 87
[27] Bernard, J.-P., Reach, W.T., Paradis, D., et al. 2008, AJ, 136, 919